

Radial Outflows in Narrow-Line Region of Seyfert Galaxies: No observational Evidence for Radio Jet Acceleration

Varendra Das & D. Michael Crenshaw

Department of Physics & Astronomy, Georgia State University, Atlanta



Abstract

We present a study of high-resolution long-slit spectra of the narrow-line regions (NLRs) of NGC 4151 and NGC 1068 obtained with the Space Telescope Imaging Spectrograph (STIS) aboard the *The Hubble Space Telescope (HST)*. The spectra of NGC 1068 were retrieved from the Multimission Archive at Space Telescope (MAST) and were originally taken by Cecil et al. in 1999 and 2000 during seven orbits of *HST* time. The spectra of NGC 4151 were also obtained from MAST and were taken by Hutchings et al. in 2000 during five orbits of *HST* time. All slits were laid out in a parallel configuration at position angles 38° (NGC 1068) and 52° (NGC 4151) and have a spatial resolution of $0''.2$ across and $0''.1$ along them. The forbidden twin [OIII] emission lines $\lambda\lambda$ 4959, 5007 were dispersed with the G430M grating at a resolving power $\lambda/\Delta\lambda$ of $\sim 9,000$, which permitted accurate measurement of radial velocities and dispersions. This high dispersion $\sim 0.5 \text{ \AA}$ allowed us to detect multiple kinematic components for each [OIII] emission line. Measurements were made using the brighter $\lambda 5007$ line. Biconical outflow models were generated to match the data and for comparison to previous models done for lower (~ 1000) dispersion observations. The general trend is an increase in radial velocity roughly proportional to distance from the nucleus followed by a linear decrease after roughly 100 parsec, similar to that seen in other Seyfert galaxies, indicating common acceleration/deceleration mechanisms.

MERLIN radio maps of the NLR of NGC 1068 from Gallimore et al. (2004) and VLA plus VLBA radio maps of the NLR of NGC 4151 from Mundell et al. (2003) were used to examine the dependency of the NLR cloud velocities on the radio structure. The bright NLR clouds showed a smooth transition and no disturbance across the radio knots in radial velocity and velocity dispersion plots. The fainter clouds however, seemed to be disturbed in the vicinity of the radio knots.

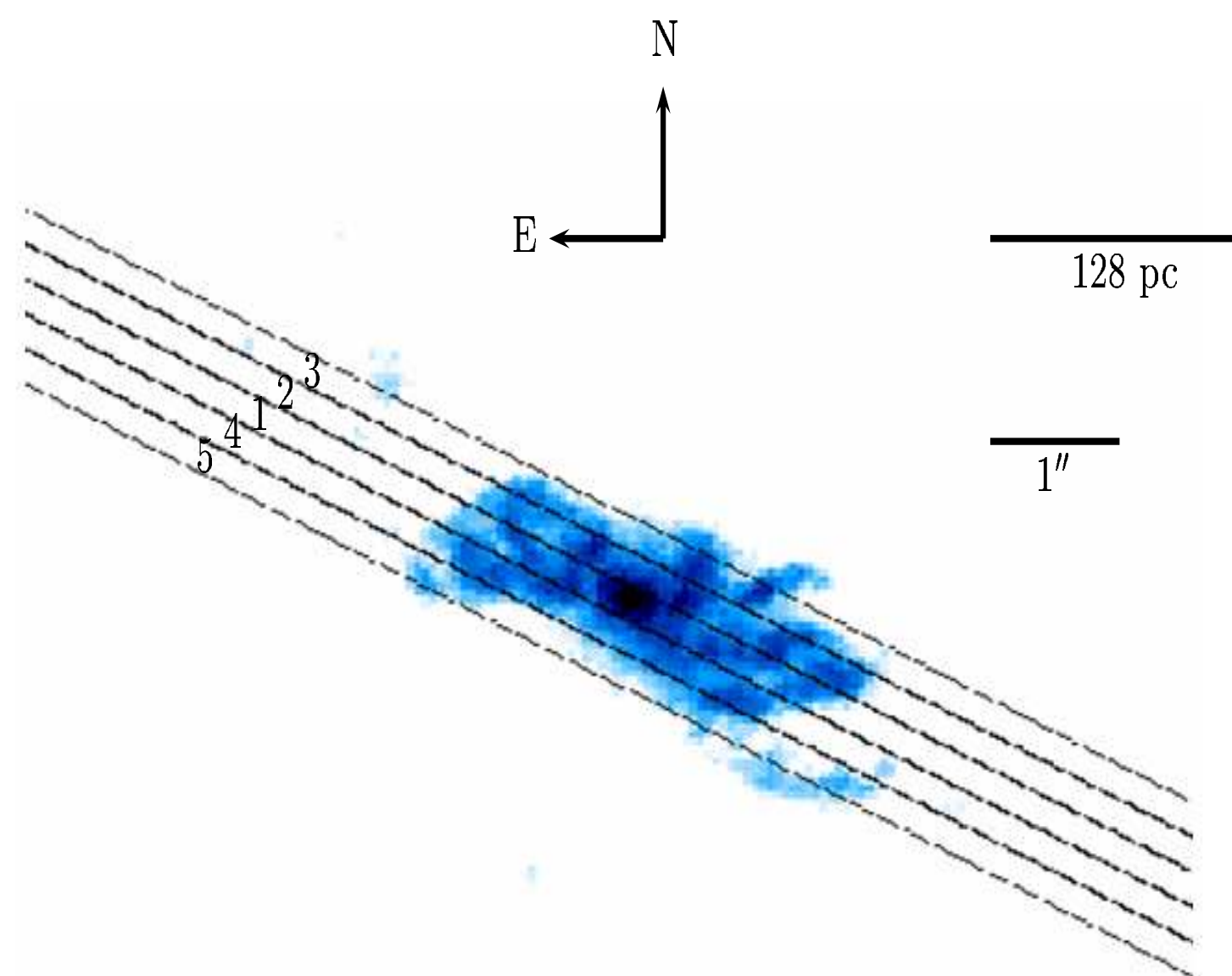


Figure 1. WFPC2 F501N image of the NLR of NGC 4151 with the 5 slits overlaid. Image courtesy of Kaiser et al. (2000).

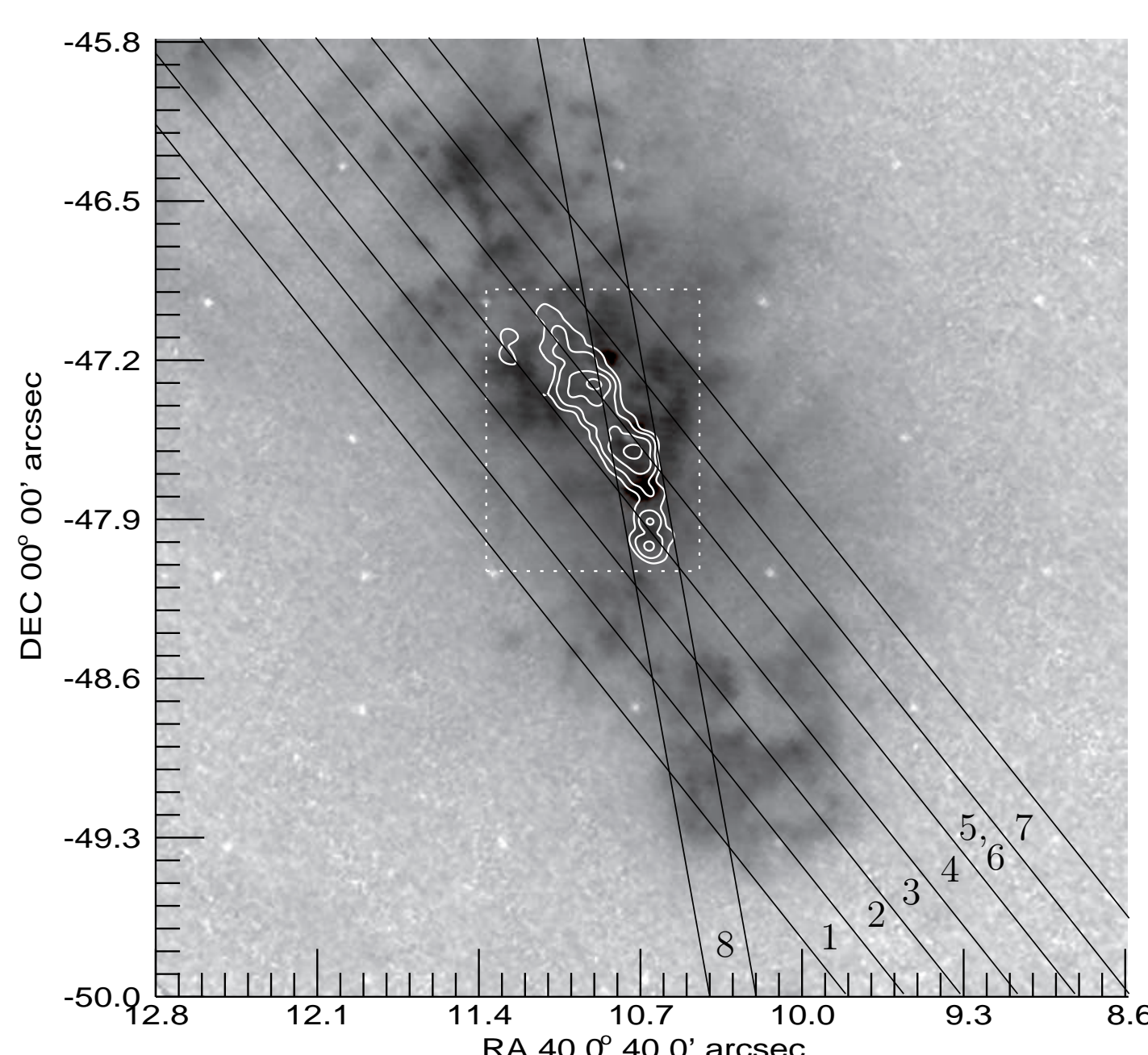


Figure 2. FOC/COSTAR 501N image of the NLR of NGC 1068 with the 8 slits overlaid. Slit 8 was taken by Antonucci et al. in 2000 January at PA 10° . The radio map is shown in white contours. Image courtesy of Macchetto et al. (1994).

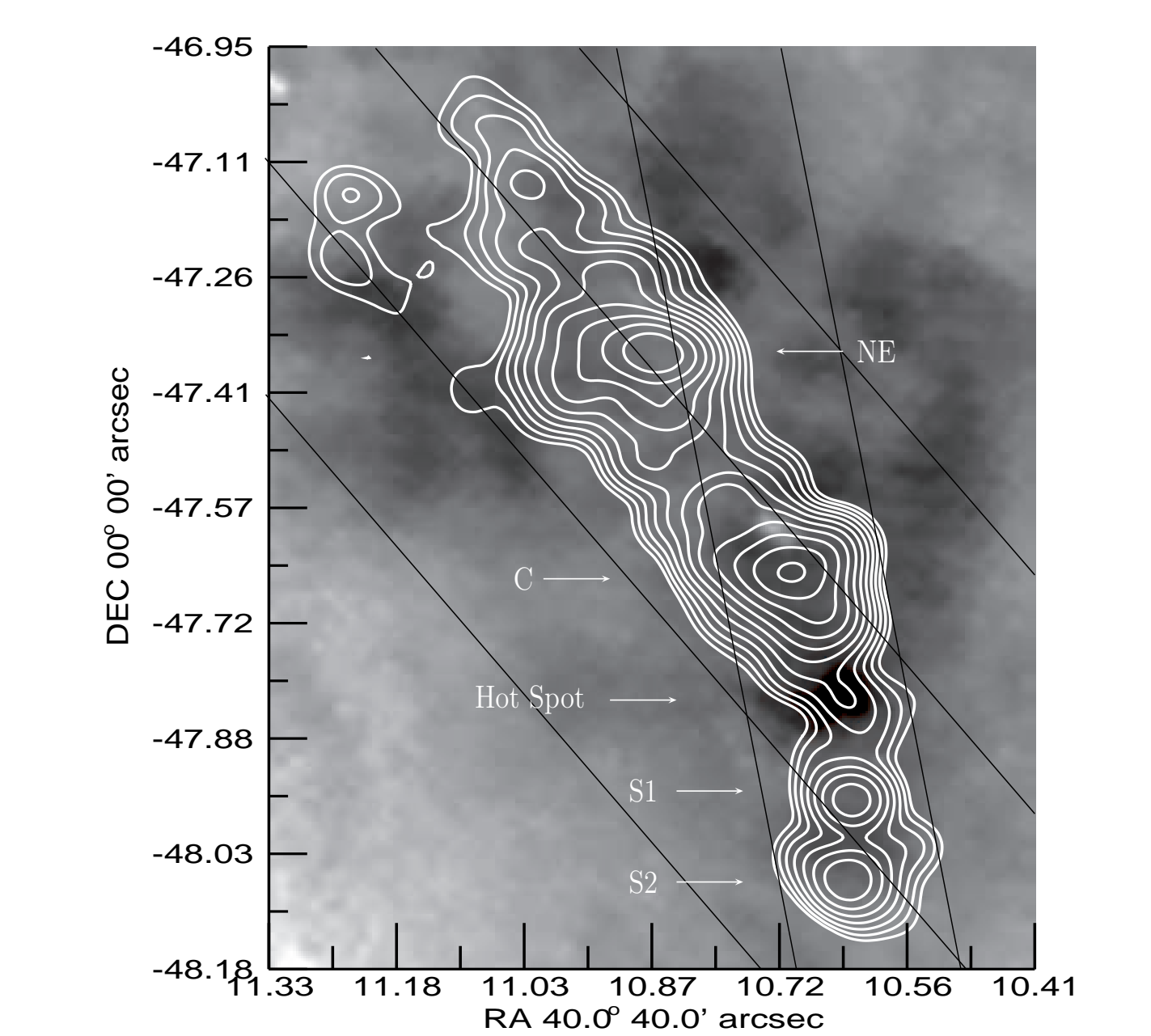


Figure 3. Blown-up version of the region enclosed in the white rectangle in Figure 2. The white letters labeled the various radio knots, and the 'hot spot' is dark spot in the center of slit 8.

Analysis

The data for NGC 4151 and NGC 1068 were analysed similarly. Each slit contained several hundred spectra containing the [OIII] doublet and $H\beta$ emission lines. Each of the [OIII] doublets contained multiple components as seen in Figure 4. We used the brighter emission line $\lambda 5007$ and fit each component with a gaussian and a continuum in order to extract their radial velocities. Radial velocities were measured using the center of each gaussian peak and by using the non-relativistic doppler formula:

$$V = c \frac{\lambda - \lambda_0}{\lambda_0} \quad (1)$$

$$V_{\text{radial}} = V - V_{\text{host systemic}} \quad (2)$$

The systemic velocities used are 1148 km s^{-1} for NGC 4151 (Brinks et al. 1997) and 997 km s^{-1} for NGC 1068 (Pedlar et al. 1992). The multiple components per spectrum were color coded red(highest flux), blue(medium flux), and black(lowest flux) to distinguish them, and they were then compared to previous low dispersion data by Crenshaw & Kraemer (2000) and Crenshaw et al. (2000). The radial velocities were then plotted versus position for each slit and compared to models.

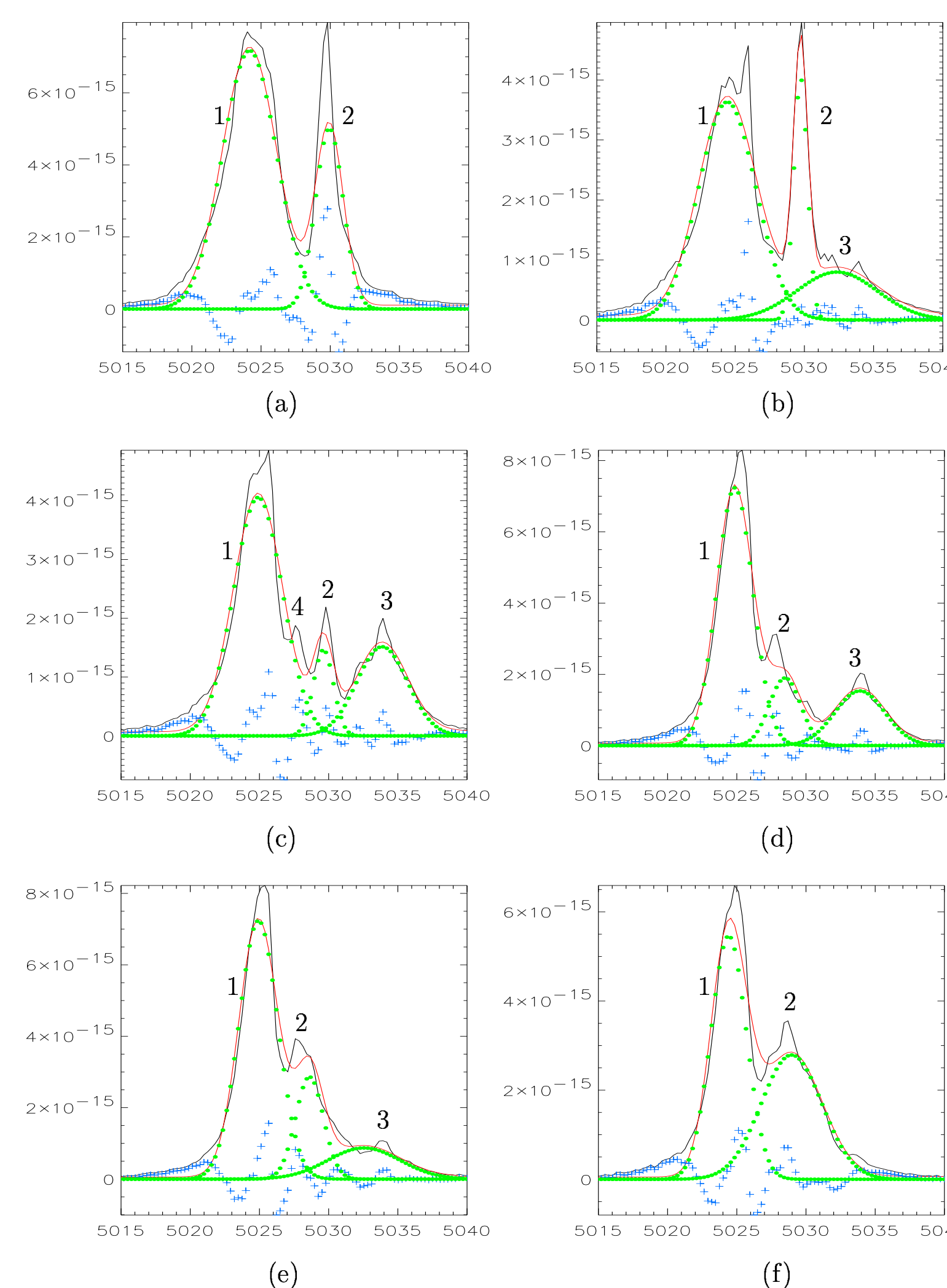
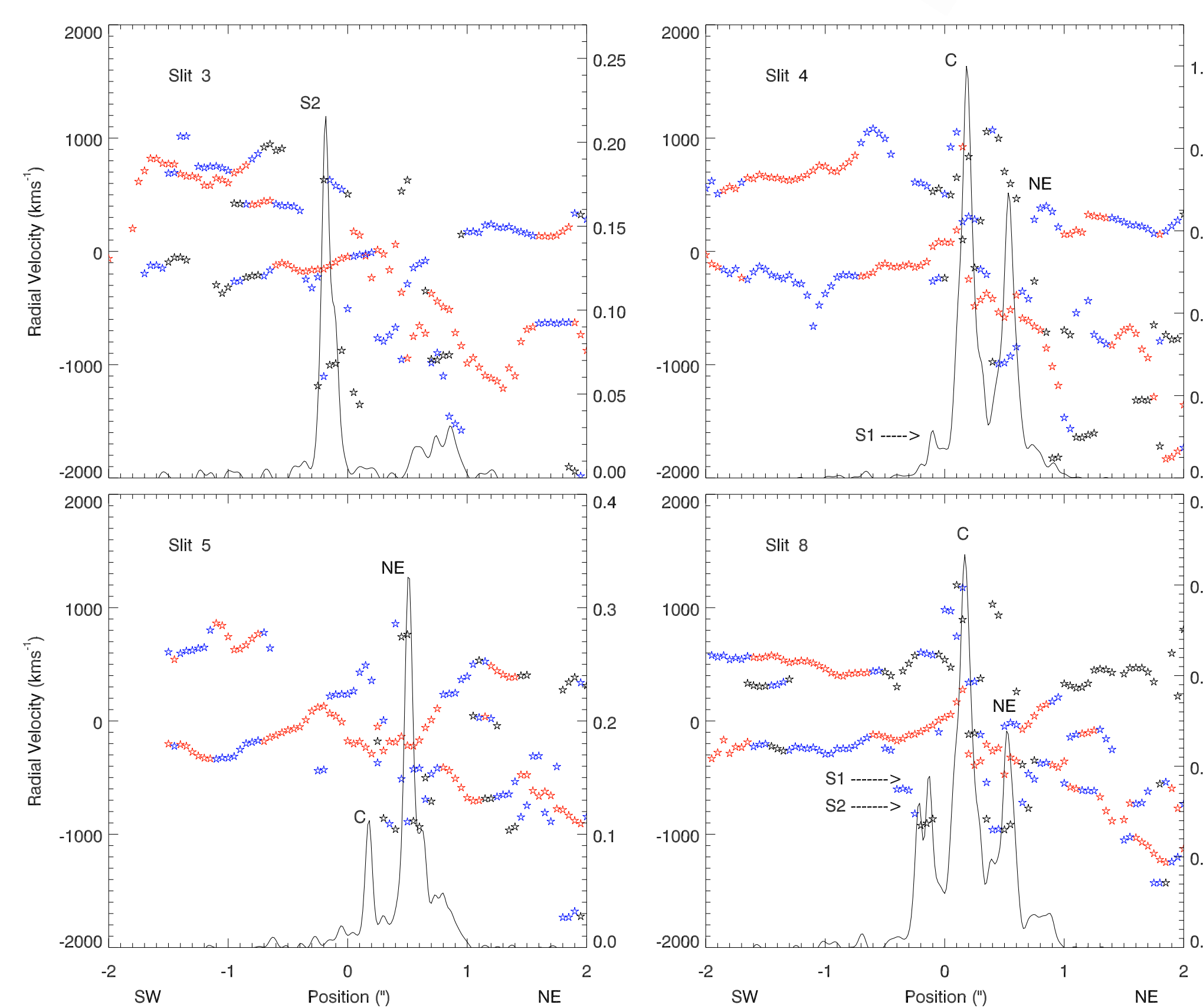


Figure 4. shows examples of multiple components detected in the spectra. These adjacent spectra were taken from the NE portion of slit 1 for NGC 4151 (see Figure 1) and cover about $0''.3$ (19 pc). The green dots are individual gaussian fits, the red is the total fit, and the blue gives the error in the fit.

We also used the high resolution radio maps from Gallimore et al. (2004) and Mundell et al. (2003) and overlaid them on the [OIII] maps provided by Macchetto et al. (1994) (NGC 1068) and Kaiser et al. (2000) (NGC 4151) to extract similar regions corresponding to the slit positions of STIS (Figures 2, 3, 5). We then made plots of radial velocities and relative radio intensities against positions along each slit that intersects the radio regions. These plots are shown in Figure 6.

Figure 5. Right:- Slit placements (that mimic those of Figure 1) on top of the radio emissions for NGC 4151.

Figure 6. Below:- Plots of spatial relative radio intensities together with radial velocities for NGC 1068.



Models

We generated a 3-D array and filled it with velocities based on a "Hubble outflow" velocity law ($V_{\text{outflow}} \propto r$). Points outside the bicone geometry were given a nonsensical velocity to distinguish them. We then convert the outflow velocities of each valid point to radial velocities, depending on its (x, y, z) coordinates. These radial velocities are then mapped to a red-blue color table in IDL to depict their redshifts or blueshifts. The parameters that we used to build the bicone are defined below.

Parameter	Symbol
Maximum extent of the bicone	z_{max} (pc)
Inner opening angle	θ_{inner} (deg)
Outer opening angle	θ_{outer} (deg)
Inclination of bicone axis	i_{axis} (deg)
Position angle of bicone axis	ϕ_{axis} (deg)
Maximum velocity ^a	v_{max} km s^{-1}
Turnover distance ^a	r_t (pc)

^a relative to nucleus

Once a model with a parameter set has been generated, we extract slits that mimic the positions, orientations, and widths with those of STIS on the source. An example of the process is shown in Figure 8. Once we have a plot such as Figure 8(d), we compared it to the radial velocity data as depicted under Model Fitting below. This comparison is done by the 'Chi by Eye' method whereby the input parameters are adjusted and the models rerun and compared to data until we determine a best fit by eye. Table 2 gives the final best fit parameter set for NGC 4151 and NGC 1068. These parameters were used to generate Figures 8 (a) and (d); note that the PA is not depicted in these images.

Model Fitting

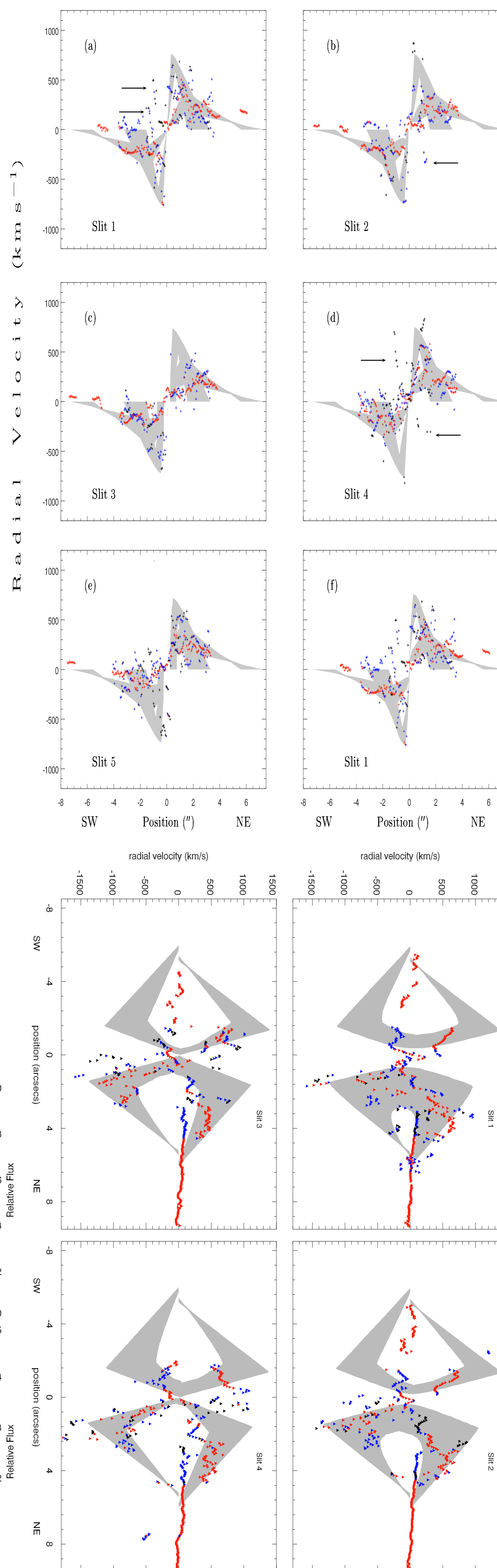


Figure 7. Fitting the models for NGC 4151 (top) and NGC 1068 (bottom).

Models

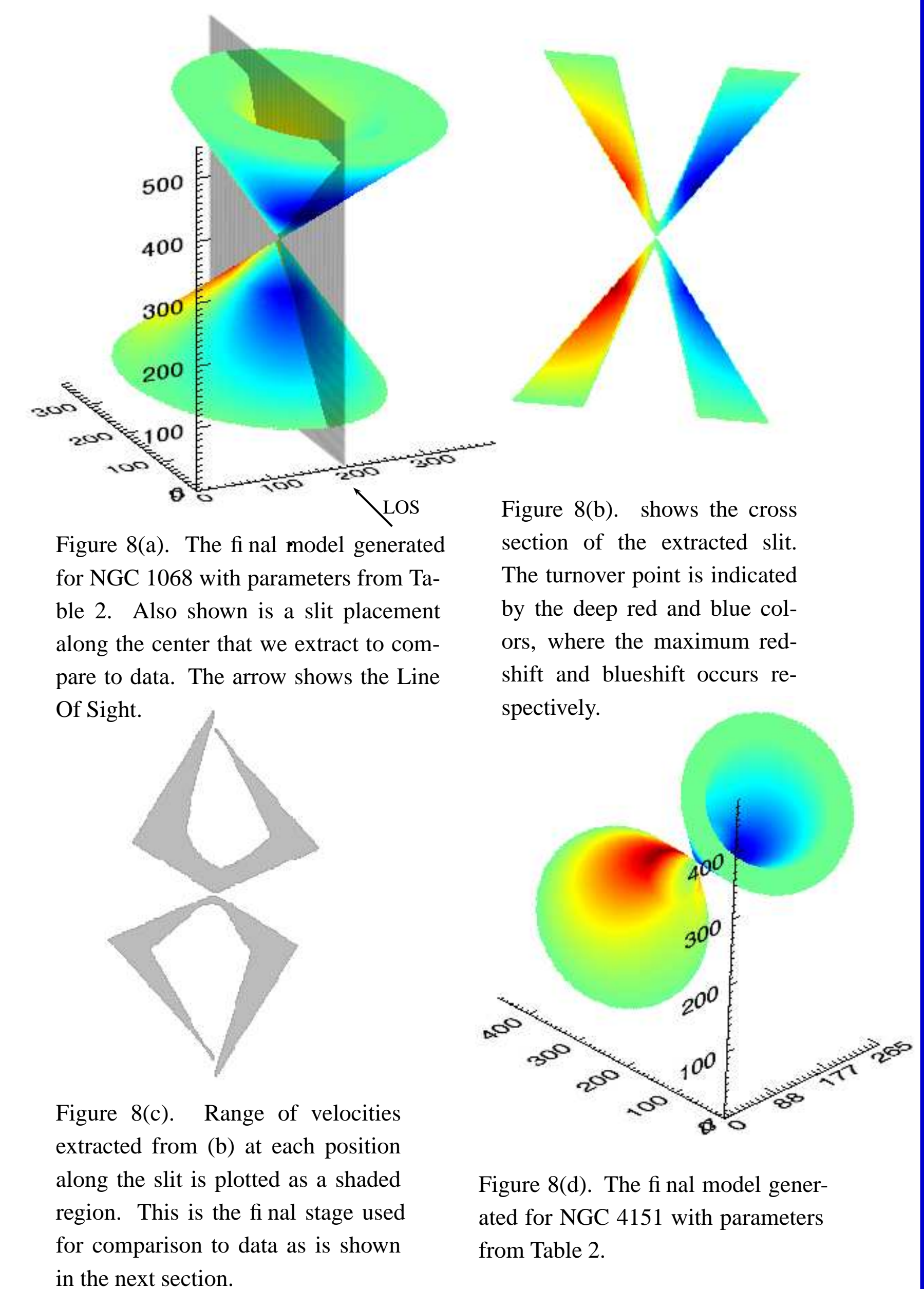


Figure 8(a). The final model generated for NGC 1068 with parameters from Table 2. Also shown is a slit placement along the center that we extract to compare to data. The arrow shows the Line Of Sight.

Figure 8(b). shows the cross section of the extracted slit. The turnover point is indicated by the deep red and blue colors, where the maximum redshift and blueshift occurs respectively.

Figure 8(c). Range of velocities extracted from (b) at each position along the slit is plotted as a shaded region. This is the final stage used for comparison to data as is shown in the next section.

Figure 8(d). The final model generated for NGC 4151 with parameters from Table 2.

Parameter	NGC 4151	NGC 1068
z_{max} (pc)	400 ± 16	400 ± 16
θ_{inner} (deg)	15 ± 2	20 ± 2
θ_{outer} (deg)	33 ± 2	40 ± 2
i_{axis} (deg)	45 ± 5^a	5 ± 2^b
ϕ_{axis} (deg)	52 ± 2	30 ± 2
v_{max} km s^{-1}	800 ± 50	2000 ± 50
r_t (pc)	96 ± 16	140 ± 16

^a Southwest is closer ^b Northeast is closer

Discussion

We confirm our previous biconical outflow models (Crenshaw et al. 2000) and (Crenshaw & Kraemer 2000) that were used to match the radial velocities of the NLR in NGC 4151 and NGC 1068, using higher velocity resolution STIS spectra. The models proved to be consistent at various position angles and across Seyfert types, except near the apex, where there are regions of [OIII] gas outside the model boundaries that fall observationally within the slit. This indicates that either 1.] the torus at the apex is patchy, allowing gas and ionizing photons to escape, or 2.] that the outflow is constrained by an entirely different somewhat larger medium.

The radio jet does not seem to cause any disturbance to the general flow of the [OIII] emission and is not directly responsible for the acceleration of the gas. Because the radio beam is much narrower than the inner opening of the bicone, there is no chance for radial acceleration by the jet, unless there is significant precession. However, the jet might be useful in clearing out a channel that coincides with our hollowed out geometry. For lateral radio jet induced acceleration to work, one should see both blue and red-shifts roughly at the same position in the case of NGC 4151, but there is no evidence for this. In NGC 1068 this lateral acceleration of the NLR clouds due to the radio jet is not seen either (see Figure 6), in this case because the bright clouds (red points) are not disturbed near the radio knots (note smooth transition). At positions in the vicinity of the radio knots however, there seemed to be clear indication that the lower luminosity clouds (blue and black points) are disturbed. These lower clouds may be ablated from the giant NLR clouds by the radio jet.

REFERENCES

- Brinks, E., Skillman, E. D., Terlevich, R. J., & Terlevich, E. 1997, *Ap&SS*, 248, 23
- Crenshaw, D. M. & Kraemer, S. B. 2000, *ApJ*, 532, L101
- Crenshaw, D. M., Kraemer, S. B., Hutchings, J. B., Bradley II, L. D., Gull, T. R., Kaiser, M. E., Nelson, C. H., Ruiz, J. R., & Weistrop, D. 2000, *ApJ*, 120, 1731
- Gallimore, J. F., Baum, S. A., & O'Dea, C. P. 2004, *ApJ*, 613, 794
- Kaiser, M. E., Bradley, L. D., Hutchings, J. B., Crenshaw, D. M., Gull, T. R., Kraemer, S. B., Nelson, C. H., Ruiz, J., & Weistrop, D. 2000, *ApJ*, 528, 260
- Macchetto, F., Capetti, A., Sparks, W. B., Axon, D. J., & Boksenberg, A. 1994, *ApJ*, 435, L15
- Mundell, C. G., Wrobel, J. M., Pedlar, A., & Gallimore, J. F. 2003, *ApJ*, 583, 192
- Pedlar, A., Howley, P., Axon, D. J., & Unger, S. W. 1992, *MNRAS*, 259, 369